Noname manuscript No.
(will be inserted by the editor)

Fully analytical solution to discrete behavior of hybrid zero dynamics in limit cycle walking with constraint on impact posture

Fumihiko Asano

Received: date / Accepted: date

Abstract This paper proposes a fully analytical solution to the discrete behavior of hybrid zero dynamics (HZD) in limit cycle walking with constraint on impact posture. First, we introduce a passive rimless wheel and explain the stability principle through derivations of the analytical transition functions of the state error for the stance and collision phases. Second, we consider an active rimless wheel driven by a steady control input for investigating the stability of semi-passive dynamic walking, and propose a method for analytically deriving the transition function for the stance phase without including unknown parameters. We then numerically investigate the solution accuracy and discuss how the discrete behavior of the HZD changes according to the control parameters. Furthermore, we extend the analysis to level walking of an underactuated rimless wheel with a torso and show that the discrete behavior of the HZD can be determined in the same manner.

Keywords Limit cycle walking · Stability · Analytical solution · Linearization · Quadratic approximation

1 Introduction

Understanding the stability principle inherent in limit-cycle walking is one of the most fundamental issues in the area of robotic efficient legged locomotion. The generated gait is mathematically described as a closed orbit with impulse effects in phase space and is a nonlinear hybrid dynamical system.

F. Asano
School of Information Science, Japan Advanced Institute of Science and Technology
1-1 Asahidai, Nomi, Ishikawa 923-1292, Japan
Tel.: +81-761-51-1243
Fax: +81-761-51-1149
E-mail: fasano@jaist.ac.jp

The self-stabilization mechanism of underactuated limit-cycle walkers [1,2] including passive-dynamic walkers [4,5] still remains to be elucidated due to the complexity of the hybrid zero dynamics (HZD) [1,3].

A rimless wheel (RW) [4,6,7] is the simplest passive-dynamic walker and its 1-DOF HZD is always asymptotically stable. This is because it automatically achieves the two necessary conditions for guaranteeing the asymptotic stability; one is the constraint on impact posture and the other is the constraint on restored mechanical energy [8,9]. The former is to make the walker fall down as a 1-DOF rigid body in a fixed posture and is the condition for maintaining the energy-loss coefficient constant. The latter is accordingly met in a passive-dynamic gait. The asymptotic stability of the discrete HZD is then easily proved by using a recurrence formula of kinetic energy immediately before impact.

An underactuated limit-cycle walker with free ankle-joints can achieve the constraint on impact posture by controlling all the active joints [10,11]. The discrete behavior of the HZD is then reduced to a 1-DOF return map and is described as a scalar transition function of the stance angular velocity at impact. Achieving the constraint on mechanical energy concurrently is not easy to be met in general unless the ankle-joint actuation is available [8,9], but it is well known that the discrete HZD in the generated gait becomes asymptotically stable in most cases.

Recently, the author proposed a method to analytically derive the scalar transition functions for the stance and collision phases [12,13]. The function for the stance phase, however, involved the steady gait parameters such as the step period and stance angular velocity at impact. This solution is a semi-analytical solution in the sense that the value cannot be calculated unless the steady parameters are obtained through numerical simulations. In addition, the need of the steady gait parameters means the unreasonableness that we can determine the stability only of a stable walking gait.

The goal of above studies is to develop a method for determining the limit cycle stability without depending on numerical integration and concerning the calculation accuracy. Based on these observations, in this paper we propose a method for deriving a fully analytical solution to discrete behavior of HZD in limit cycle walking with constraint on impact posture. We show that the transition function of the state error for the stance phase can be analytically derived by using linearly-approximated equation of motion and quadratically-approximated mechanical energy. By using the transition functions derived, we can instantaneously determine the stability of HZD and discrete behavior of the gait to be generated without performing numerical simulations.

This paper is organized as follows. From Section 2 to Section 4, we discuss the discrete behaviors of 1-DOF passive and semi-passive dynamic walkers to clearly explain the method. Section 2 describes the stability principle underlying passive dynamic walking of a RW. Section 3 introduces a 1-DOF active RW model for analysis and describes the linearized equation of motion and quadratic approximation of mechanical energy. Section 4 derives the analytical transition function of the state error for the stance phase and discusses its

accuracy through numerical simulations. Section 5 extends the analysis to an underactuated RW model and describes the method in general cases. Finally, Section 6 concludes this paper and describes future research direction.

2 Stability of 1-DOF passive dynamic walking

2.1 Passive rimless wheel model

In this section, we consider the RW model shown in Fig. 1. This model is planar and eight-legged. The radius or leg length is l [m] and the total mass is m [kg]. The angle between two adjacent leg frames is α and is $\pi/4$ [rad]. We assume that the model does not have inertia moment and the contact point with the ground does not slip during motion. Let θ [rad] be the angular position of the stance leg with respect to vertical. The kinetic energy, K [J], and the potential energy, P [J], then become

$$K(\dot{\theta}) = \frac{1}{2}ml^2\dot{\theta}^2, \quad P(\theta) = mgl\cos\theta. \tag{1}$$

Following Lagrange's method, the equation of motion becomes

$$ml^2\ddot{\theta} - mgl\sin\theta = 0. \tag{2}$$

In the following, we describe the collision dynamics. Before it, we define the basic terms and notations.

– Let the subscript "i" be the number of steps and $i \geq 0$.

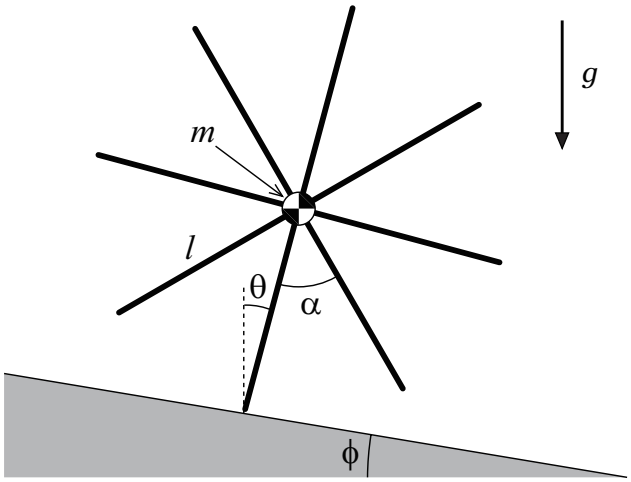

Fig. 1 Passive rimless wheel model

– The walker starts walking from an impact posture; this is defined as the (0)th impact. The next impact is the (1)st impact, and the motion between the (0)th and the (1)st impacts is called the (0)th step. The subsequent impacts and steps are contextually counted.
– The superscripts "−" and "+" denote immediately before and immediately after impact.
– The subscript "eq" denotes that the parameter is at the equilibrium point on the Poincaré section.
– The superscript "∗" denotes that the parameter is of the stationary orbit.

The relation between the angular velocity immediately before the (i)th impact and that immediately after the (i)th impact is given by

$$\dot{\theta}_i^+ = \cos\alpha \cdot \dot{\theta}_i^- . \tag{3}$$

See [14] for the detailed derivation. Let ϕ [rad] be the slope angle. Then the angular positions immediately before and immediately after impact are always

$$\theta_i^\pm = \theta_{\mathrm{eq}}^\pm = \phi \mp \frac{\alpha}{2}, \tag{4}$$

and their errors are thus always zeros.

2.2 Poincaré return map

It has already been known that the generated passive gait of a RW always becomes 1-period asymptotically stable because it always falls down as a 1-DOF rigid body and the energy-loss coefficient and restored mechanical energy are automatically kept constant. In the following, we outline the stability principle.

Let K_i^- [J] be the kinetic energy immediately before the (i)th impact. Then the following recurrence formula holds.

$$K_{i+1}^- = \varepsilon K_i^- + \Delta E \tag{5}$$

Where ε [-] is the energy-loss coefficient which is determined as

$$\varepsilon := \frac{K_i^+}{K_i^-} = \frac{\frac{1}{2}ml^2\left(\dot{\theta}_i^+\right)^2}{\frac{1}{2}ml^2\left(\dot{\theta}_i^-\right)^2} = \left(\frac{\dot{\theta}_i^+}{\dot{\theta}_i^-}\right)^2 = \cos^2\alpha. \tag{6}$$

ΔE [J] is the restored mechanical energy by gravity and is determined as

$$\Delta E = 2mgl\sin\frac{\alpha}{2}\sin\phi. \tag{7}$$

Both ε and ΔE are positive constants. Following Eq. (5), K_i^- converges to

$$K_{\mathrm{eq}}^- := \lim_{i\to\infty} K_i^- = \frac{\Delta E}{1-\varepsilon}. \tag{8}$$

This gives the proof of the asymptotic stability. In a steady gait, the following equation holds.

$$K_{\mathrm{eq}}^{-} = \varepsilon K_{\mathrm{eq}}^{-} + \Delta E \tag{9}$$

K_i^- can be approximated as follows.

$$\begin{aligned} K_i^- &= \frac{1}{2}ml^2\left(\dot{\theta}_i^-\right)^2 = \frac{1}{2}ml^2\left(\dot{\theta}_{\mathrm{eq}}^- + \Delta\dot{\theta}_i^-\right)^2 \approx \frac{1}{2}ml^2\left(\dot{\theta}_{\mathrm{eq}}^-\right)^2 + ml^2\dot{\theta}_{\mathrm{eq}}^-\Delta\dot{\theta}_i^- \\ &= K_{\mathrm{eq}}^- + ml^2\dot{\theta}_{\mathrm{eq}}^-\Delta\dot{\theta}_i^- \end{aligned} \tag{10}$$

In the same way, K_{i+1}^- becomes

$$K_{i+1}^- \approx K_{\mathrm{eq}}^- + ml^2\dot{\theta}_{\mathrm{eq}}^-\Delta\dot{\theta}_{i+1}^-. \tag{11}$$

By substituting Eqs. (10) and (11) into Eq. (9), we get

$$K_{\mathrm{eq}}^- + ml^2\dot{\theta}_{\mathrm{eq}}^-\Delta\dot{\theta}_{i+1}^- = \varepsilon\left(K_{\mathrm{eq}}^- + ml^2\dot{\theta}_{\mathrm{eq}}^-\Delta\dot{\theta}_i^-\right) + \Delta E. \tag{12}$$

By subtracting Eq. (9) from Eq. (12), we finally get

$$\Delta\dot{\theta}_{i+1}^- = \varepsilon\Delta\dot{\theta}_i^-. \tag{13}$$

The angular velocity error therefore converges to zero at a constant rate, ε, as the walking motion continues. This shows that the HZD of the RW, the overall behavior of the stance-leg angle, is asymptotically stable.

2.3 Stability of collision phase

We can rearrange Eq. (3) considering the error term as

$$\dot{\theta}_{\mathrm{eq}}^+ + \Delta\dot{\theta}_i^+ = \cos\alpha\left(\dot{\theta}_{\mathrm{eq}}^- + \Delta\dot{\theta}_i^-\right). \tag{14}$$

In a steady gait, Eq. (3) becomes

$$\dot{\theta}_{\mathrm{eq}}^+ = \cos\alpha\cdot\dot{\theta}_{\mathrm{eq}}^-. \tag{15}$$

By subtracting Eq. (15) from Eq. (14), we get

$$\Delta\dot{\theta}_i^+ = \cos\alpha\cdot\Delta\dot{\theta}_i^-. \tag{16}$$

In the following, we denote the transition function as $\bar{R} = \cos\alpha$. In addition, following Eq. (14), this is also specified as the ratio of the steady angular velocities:

$$\bar{R}^2 = \left(\frac{\dot{\theta}_i^+}{\dot{\theta}_i^-}\right)^2 = \left(\frac{\dot{\theta}_{\mathrm{eq}}^+}{\dot{\theta}_{\mathrm{eq}}^-}\right)^2 = \varepsilon. \tag{17}$$

2.4 Stability of stance phase

Let us assume that the transition function of the state error during the stance phase is specified as

$$\Delta\dot{\theta}_{i+1}^{-} = \bar{Q}\Delta\dot{\theta}_{i}^{+}. \tag{18}$$

Following Eqs. (14) and (18), the transition function, $\bar{Q}$, is then solved as

$$\bar{Q} = \frac{\varepsilon}{\bar{R}} = \cos\alpha. \tag{19}$$

Therefore, we can find that the transition of the state error during the stance and collision phases are identical and are $\cos\alpha$. In the subsequent sections, we will investigate this result in more detail from the mechanical energy point of view.

3 Preliminary to analysis of semi-passive dynamic walking

3.1 Active combined rimless wheel model and linearization of motion

As the realistic model of an active 1-DOF limit-cycle walker, we consider an active combined rimless wheel (CRW) shown in Fig. 2 [15]. This is composed of two identical eight-legged RWs of Fig. 1 and a body frame, and can exert a joint torque, u [N·m], between the rear stance-leg and the body frame. We assume the following statements.

- The fore and rear stance legs always contact with the ground without sliding.
- The inertia moments about the CoMs of all the frames can be neglected.
- The rear and fore RWs perfectly synchronize or rotate maintaining the relation $\theta_r \equiv \theta_f$.

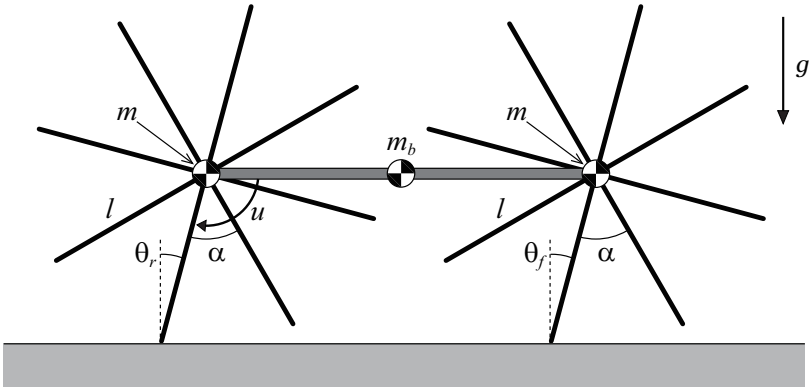

Fig. 2 Active combined rimless wheel model

The 3-DOF CRW with the hard ground configurates a four-bar linkage, and exerting the joint torque, u, is thus equivalent to exerting that at the contact point with the ground (ankle-joint torque). The dynamics of the rear RW then becomes identical to that of an active RW with an ankle-joint torque, that is,

$$Ml^2\ddot{\theta} - Mgl\sin\theta = u \tag{20}$$

where $M := m_b + 2m$ [kg] is the total mass of the CRW and $\theta := \theta_r = \theta_f$ is the stance-leg angle. By linearizing this around $\theta = \dot{\theta} = 0$, Eq. (20) becomes

$$Ml^2\ddot{\theta} - Mgl\theta = u, \tag{21}$$

and the state-space realization of the reduced CRW dynamics becomes

$$\frac{\mathrm{d}}{\mathrm{d}t}\begin{bmatrix}\theta\\ \dot{\theta}\end{bmatrix} = \begin{bmatrix}0 & 1\\ \omega^2 & 0\end{bmatrix}\begin{bmatrix}\theta\\ \dot{\theta}\end{bmatrix} + \begin{bmatrix}0\\ 1/Ml^2\end{bmatrix}u, \tag{22}$$

where $\omega := \sqrt{g/l}$ [1/s]. We denote Eq. (22) as

$$\dot{\boldsymbol{x}} = \boldsymbol{A}\boldsymbol{x} + \boldsymbol{B}u. \tag{23}$$

The linearized CRW dynamics is formulated a linear time-invariant system with one control input, and is identical to that of the single RW. We then call it simply RW in the following.

The transition function for the collision phase, $\bar{R}$, in this case also becomes identical to that of the passive single RW, Eq. (16). We again use $\bar{R}$ without applying linearization or quadratic approximation.

The active RW can walk on level ground by exerting the control input, u [15]. In this paper, however, we apply slight actuation to the passive RW on a slope for investigating how the convergence property changes from natural one.

3.2 Quadratic approximation of mechanical energy

The kinetic energy of the original (nonlinear) RW is determined as

$$K(\dot{\theta}) = \frac{1}{2}Ml^2\dot{\theta}^2, \tag{24}$$

and the corresponding one to the linearized model is identical to this. Whereas the potential energy for the original RW is determined as $P(\theta) = Mgl\cos\theta$ [J], and we consider its quadratic approximation

$$P(\theta) = Mgl\left(1 - \frac{\theta^2}{2}\right), \tag{25}$$

Let us define Eq. (25) as the potential energy corresponding to the linearized system in the sense that this leads to the dynamic equation of Eq. (21) together with $K(\dot{\theta})$. In addition, let us define the maximum potential energy, $P_{\max} :=$

Mgl [J]; this is the maximum potential energy the robot can reach during the stance phases. Eq. (25) is then rewritten as follows.

$$P(\theta) = P_{\max} - \frac{1}{2}Mgl\theta^2 \tag{26}$$

The total mechanical energy is then determined as

$$E(\boldsymbol{x}) = P_{\max} + \frac{1}{2}\boldsymbol{x}^{\mathrm{T}}\boldsymbol{W}_0\boldsymbol{x}, \tag{27}$$

where

$$\boldsymbol{W}_0 := \begin{bmatrix} -Mgl & 0 \\ 0 & Ml^2 \end{bmatrix} \tag{28}$$

is a constant matrix including the inertia and gravity.

The following equation

$$\frac{\mathrm{d}}{\mathrm{d}t}\frac{\partial K(\dot{\theta})}{\partial \dot{\theta}} - \frac{\partial K(\dot{\theta})}{\partial \theta} + \frac{\partial P(\theta)}{\partial \theta} = 0 \tag{29}$$

derived by using Eqs. (24) and (25) becomes identical to the linearized dynamic equation (21).

The time-derivative of $E(\boldsymbol{x})$ becomes

$$\frac{\mathrm{d}E(\boldsymbol{x})}{\mathrm{d}t} = \boldsymbol{x}^{\mathrm{T}}\boldsymbol{W}_0\dot{\boldsymbol{x}} = \boldsymbol{x}^{\mathrm{T}}\boldsymbol{W}_0\left(\boldsymbol{A}\boldsymbol{x} + \boldsymbol{B}u\right) = \boldsymbol{x}^{\mathrm{T}}\boldsymbol{W}_0\boldsymbol{A}\boldsymbol{x} + \boldsymbol{x}^{\mathrm{T}}\boldsymbol{W}_0\boldsymbol{B}u. \tag{30}$$

Here, the product $\boldsymbol{W}_0\boldsymbol{A}$ has the form

$$\boldsymbol{W}_0\boldsymbol{A} = Ml^2\begin{bmatrix} 0 & -\omega^2 \\ \omega^2 & 0 \end{bmatrix} \tag{31}$$

and is skew-symmetric. Therefore, $\boldsymbol{x}^{\mathrm{T}}\boldsymbol{W}_0\boldsymbol{A}\boldsymbol{x} = 0$ always holds during the stance phases and Eq. (30) becomes

$$\frac{\mathrm{d}E(\boldsymbol{x})}{\mathrm{d}t} = \boldsymbol{x}^{\mathrm{T}}\boldsymbol{W}_0\boldsymbol{B}u = \dot{\theta}u. \tag{32}$$

Therefore, $E(\boldsymbol{x})$ reproduces the principle of conservation of energy in the linearized walking system.

3.3 Condition for overcoming potential barrier

Since the impact posture is always the same, that is, $\theta_i^{\pm} = \theta_{\mathrm{eq}}^{\pm}$, the following equations hold.

$$P_i^{\pm} = P_{\max} - \frac{1}{2}Mgl\left(\theta_i^{\pm}\right)^2 = P_{\max} - \frac{1}{2}Mgl\left(\theta_{\mathrm{eq}}^{\pm}\right)^2 = P_{\mathrm{eq}}^{\pm} \tag{33}$$

Eq. (33) shows that the potential energies immediately before and immediately after impact are constant values. Following Eqs. (4) and (33), the restored mechanical energy during the stance phase can be derived as

$$\Delta E = P_{\mathrm{eq}}^{+} - P_{\mathrm{eq}}^{-} = \frac{1}{2} Mgl \left(\left(\theta_{\mathrm{eq}}^{-}\right)^2 - \left(\theta_{\mathrm{eq}}^{+}\right)^2 \right) = Mgl\alpha\phi. \tag{34}$$

The steady kinetic energy immediately before impact also becomes

$$K_{\mathrm{eq}}^{-} = \frac{\Delta E}{1-\varepsilon} = \frac{Mgl\alpha\phi}{\sin^2\alpha}. \tag{35}$$

Note that, as previously mentioned, we do not linearize the collision phase and ε used in Eq. (35) is thus $\cos^2\alpha$.

A potential barrier exists during the stance phase in the case that the following inequality holds.

$$\theta_{\mathrm{eq}}^{+} = -\frac{\alpha}{2} + \phi < 0 \tag{36}$$

To overcome the potential barrier, the following inequality must be satisfied.

$$E_{\mathrm{eq}}^{\pm} - P_{\max} = K_{\mathrm{eq}}^{-} + P_{\mathrm{eq}}^{-} - P_{\max} = \frac{Mgl\alpha\phi}{\sin^2\alpha} - \frac{Mgl}{2}\left(\phi + \frac{\alpha}{2}\right)^2 > 0 \tag{37}$$

This can be solved as

$$\frac{\alpha}{2}\tan^2\frac{\alpha}{2} < \phi < \frac{\alpha}{2}\cot^2\frac{\alpha}{2}. \tag{38}$$

By summarizing Eqs. (36) and (38), the condition necessary for overcoming the potential barrier is finally specified as

$$\frac{\alpha}{2}\tan^2\frac{\alpha}{2} < \phi < \frac{\alpha}{2}. \tag{39}$$

As Eq. (35) implies, the steady walking speed monotonically increases as the slope angle, ϕ, increases. Therefore the vertical (normal) ground reaction force becomes negative during the stance phases with a steep slope angle. In other words, the condition for unilateral constraint while walking cannot be met with a steep slope angle. This always appears before the slope angle reaches $\alpha/2$. Therefore, the upper bound of Eq. (39) is conservative.

3.4 Numerical example

Fig. 3 shows the trajectories of the generated steady passive-dynamic gaits of the nonlinear and linearized models where $M = 1.0$ [kg], $l = 1.0$ [m], and $\phi = 0.10$ [rad]. We can confirm that both trajectories are similar and the linear approximation is thus valid. Fig. 4 shows the time evolution of $E(\boldsymbol{x})$. The RW started passive dynamic walking from the impact posture with the initial angular velocity of $\dot{\theta}_0^{-} = 2.0$ [rad/s], but the figure shows $E(\boldsymbol{x})$ since immediately after the (0)th impact. We can see that the value is kept

constant during the stance phases and discontinuously changes at the collision phases. The principle of conservation of mechanical energy is reproduced in the linearized system. Fig. 5 plots the evolution of the state errors, $\left|\Delta\dot{\theta}_i^-\right|$ and $\left|\Delta\dot{\theta}_i^+\right|$, with respect to the step number corresponding to Fig. 4. We can see that, as explained in Section 2, the error norm monotonically decreases during both phases at a constant rate of $\cos\alpha$. It finally converges to zero with the convergence of the linearized mechanical energy in Fig. 4.

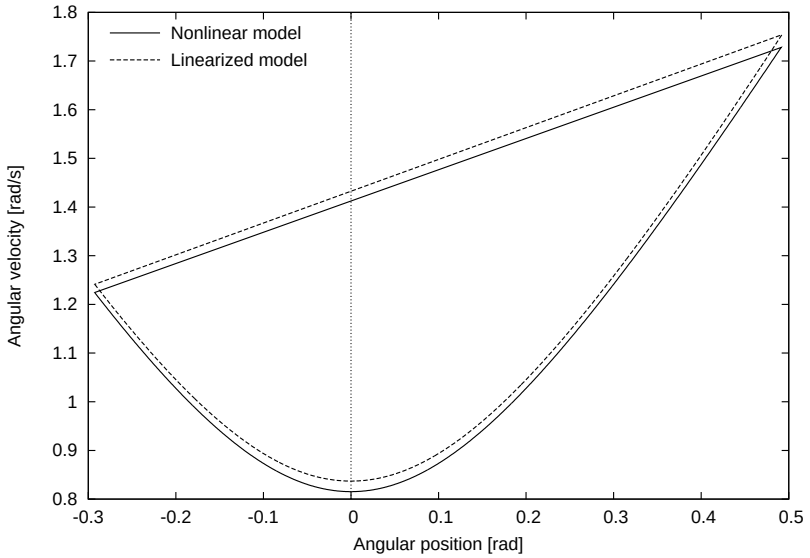

Fig. 3 Trajectories of steady gaits of nonlinear and linearized models in phase space

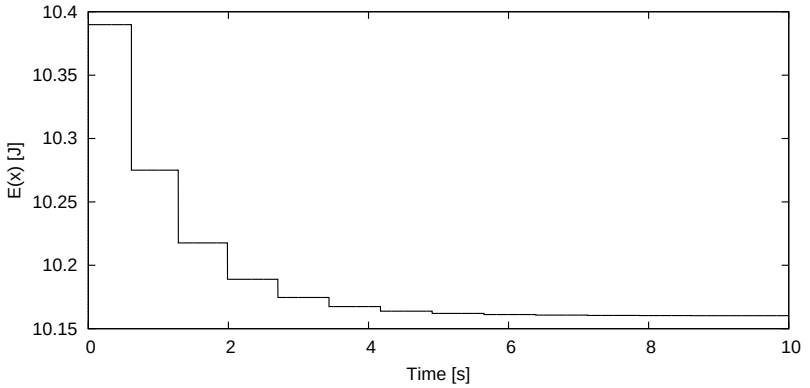

Fig. 4 Time evolution of $E(\boldsymbol{x})$

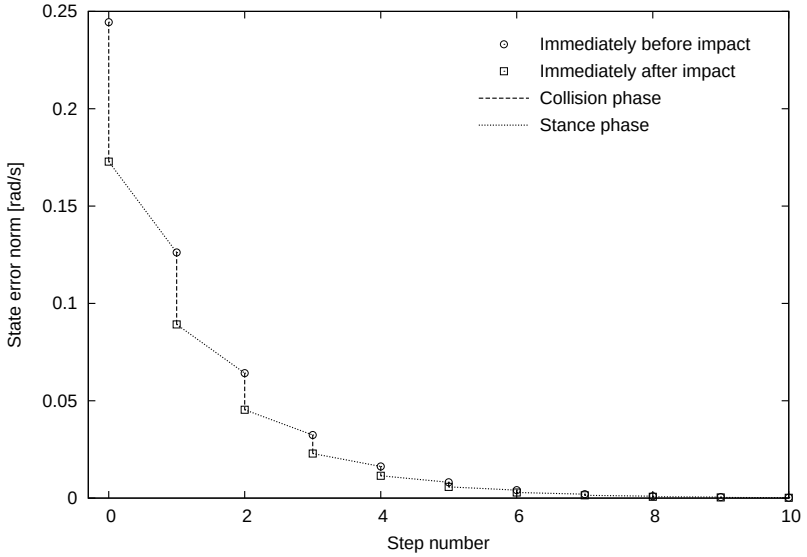

Fig. 5 Evolution of state error with respect to step number in passive-dynamic gait of Fig. 4

4 Stability of 1-DOF semi-passive dynamic walking

4.1 Problem formulation

In this paper, we define semi-passive dynamic walking as the walking gait driven by the following control input.

$$u(t) = \begin{cases} u_0 & (0 \leq t < T_{\rm set}) \\ 0 & (t \geq T_{\rm set}) \end{cases} \tag{40}$$

Here, t [s] is the time parameter and is reset to zero at every impact. $T_{\rm set}$ [s] is the desired ending time of the actuation. We assume that $T_{\rm set}$ is always shorter than the step period, that is, the actuation is terminated before the next impact. The stance-leg angle of the CRW, θ, then behaves as the HZD. A linear time-invariant system with a steady control input, u, is the unified formulation of limit cycle walking with constraint on impact posture this paper discusses. As described in the next section, general walkers can also be formulated in the same manner.

In 1-DOF semi-passive dynamic walking, the kinetic energy immediately before impact satisfies the following recurrence formula:

$$K_{i+1}^{-} = \varepsilon K_i^{-} + \Delta E_i, \tag{41}$$

where ε is the same as in Eq. (6) and ΔE_i [J] is the restored mechanical energy in the (i)th step. The problem in this case is that the restored mechanical

energy, ΔE_i, is not constant and changes at every step. In the following, we show that ΔE_i can be analytically derived as a function of $\dot{\theta}_i^-$ or $\Delta\dot{\theta}_i^-$.

4.2 Restored mechanical energy

The mechanical energy restored by the control input and gravity effect during the (i)th step becomes

$$\Delta E_i = \int_{0^+}^{T_{\rm set}} \dot{\theta}(s) u_0 \, \mathrm{d}s + Mgl\alpha\phi = \left(\theta(T_{\rm set}) - \theta_{\rm eq}^+\right) u_0 + Mgl\alpha\phi. \tag{42}$$

ΔE_i can be obtained if $\theta(T_{\rm set})$ is analytically derived. $\theta(t)$ can be analytically determined by using linear approximation. The steady state vector at t of Eq. (23), $\boldsymbol{x}(t)$, becomes

$$\boldsymbol{x}(t) = \mathrm{e}^{\boldsymbol{A}t}\boldsymbol{x}_i^+ + \int_{0^+}^{t} \mathrm{e}^{\boldsymbol{A}(t-s)}\boldsymbol{B} u_0 \, \mathrm{d}s. \tag{43}$$

By extracting the first row from $\boldsymbol{x}(t)$ and replacing t with $T_{\rm set}$, we get

$$\theta(T_{\rm set}) = \frac{\left(\cosh\left(\omega T_{\rm set}\right) - 1\right) u_0}{M\omega^2 l^2} + \theta_{\rm eq}^+ \cosh\left(\omega T_{\rm set}\right) + \frac{\dot{\theta}_i^+ \sinh\left(\omega T_{\rm set}\right)}{\omega}. \tag{44}$$

By considering the relation $\dot{\theta}_i^+ = \dot{\theta}_{\rm eq}^+ + \Delta\dot{\theta}_i^+$, Eq. (44) is arranged to

$$\theta(T_{\rm set}) = \theta^*(T_{\rm set}) + \frac{\Delta\dot{\theta}_i^+ \sinh\left(\omega T_{\rm set}\right)}{\omega}, \tag{45}$$

where

$$\theta^*(T_{\rm set}) = \frac{\left(\cosh\left(\omega T_{\rm set}\right) - 1\right) u_0}{M\omega^2 l^2} + \theta_{\rm eq}^+ \cosh\left(\omega T_{\rm set}\right) + \frac{\dot{\theta}_{\rm eq}^+ \sinh\left(\omega T_{\rm set}\right)}{\omega} \tag{46}$$

is the value of Eq. (44) in the stationary orbit. We can understand that $\theta(T_{\rm set})$ is a linear function of $\Delta\dot{\theta}_i^+$. By considering Eq. (16), Eq. (45) can be arranged to

$$\theta(T_{\rm set}) = \theta^*(T_{\rm set}) + \frac{\Delta\dot{\theta}_i^- \cos\alpha \sinh\left(\omega T_{\rm set}\right)}{\omega}. \tag{47}$$

Therefore, we can understand that $\theta(T_{\rm set})$ is a linear function of $\Delta\dot{\theta}_i^-$ and so is ΔE_i. The steady restored mechanical energy, ΔE^*, is defined and specified as

$$\begin{aligned} \Delta E^* &:= \lim_{i\to\infty} \Delta E_i = \int_{0^+}^{T_{\rm set}} \dot{\theta}^*(s) u_0 \, \mathrm{d}s + Mgl\alpha\phi \\ &= \left(\theta^*(T_{\rm set}) - \theta_{\rm eq}^+\right) u_0 + Mgl\alpha\phi. \end{aligned} \tag{48}$$

Following Eqs. (47) and (48), ΔE_i of Eq. (42) is finally arranged to

$$\Delta E_i = \Delta E^* + \frac{u_0 \cos\alpha \sinh\left(\omega T_{\rm set}\right)}{\omega} \Delta\dot{\theta}_i^-. \tag{49}$$

4.3 Poincaré return map

As is the case in passive dynamic walking, the kinetic energy immediately before impact can be approximated as

$$K_{i+1}^{-} \approx K_{\mathrm{eq}}^{-} + Ml^2\dot{\theta}_{\mathrm{eq}}^{-}\Delta\dot{\theta}_{i+1}^{-}, \tag{50}$$

$$K_{i}^{-} \approx K_{\mathrm{eq}}^{-} + Ml^2\dot{\theta}_{\mathrm{eq}}^{-}\Delta\dot{\theta}_{i}^{-}. \tag{51}$$

In a steady gait, Eq. (41) should converge to

$$K_{\mathrm{eq}}^{-} = \varepsilon K_{\mathrm{eq}}^{-} + \Delta E^{*}. \tag{52}$$

By substituting Eqs. (49), (50) and (51) into Eq. (41) and subtracting Eq. (52) from it, we get

$$Ml^2\dot{\theta}_{\mathrm{eq}}^{-}\Delta\dot{\theta}_{i+1}^{-} = \varepsilon Ml^2\dot{\theta}_{\mathrm{eq}}^{-}\Delta\dot{\theta}_{i}^{-} + \frac{u_0\cos\alpha\sinh\left(\omega T_{\mathrm{set}}\right)}{\omega}\Delta\dot{\theta}_{i}^{-}. \tag{53}$$

This equation specifies the transition of the state error from immediately before the (i)th impact to the immediately before the $(i+1)$th impact, and can be arranged to

$$\Delta\dot{\theta}_{i+1}^{-} = \bar{Q}\bar{R}\Delta\dot{\theta}_{i}^{-}, \tag{54}$$

where

$$\bar{Q}\bar{R} = \varepsilon + \frac{u_0\cos\alpha\sinh\left(\omega T_{\mathrm{set}}\right)}{M\omega l^2\dot{\theta}_{\mathrm{eq}}^{-}}. \tag{55}$$

Here, by considering Eq. (17), $\bar{Q}$ can be derived as

$$\bar{Q} = \bar{R} + \frac{u_0\sinh\left(\omega T_{\mathrm{set}}\right)}{M\omega l^2\dot{\theta}_{\mathrm{eq}}^{-}}. \tag{56}$$

By using Eq. (3), this can be arranged to

$$\bar{Q} = \bar{R} + \frac{u_0\cos\alpha\sinh\left(\omega T_{\mathrm{set}}\right)}{M\omega l^2\dot{\theta}_{\mathrm{eq}}^{+}}. \tag{57}$$

Eq. (56) or (57) describe the relationship between $\bar{Q}$ and $\bar{R}$; the stability of the stance phase is determined by that of the collision phase and the control input. If u_0 is negative, then $\bar{Q}$ becomes smaller than $\bar{R}$ $(=\cos\alpha)$ because $\dot{\theta}_{\mathrm{eq}}^{\pm}$ is always positive. Deceleration makes the convergence speed faster, and acceleration has the opposite effect. In addition, we can reconfirm the convergence property in the passive RW, $\bar{Q} = \bar{R} = \cos\alpha$, by putting $u_0 = 0$ or $T_{\mathrm{set}} = 0$.

4.4 Analytical solution of $\dot{\theta}_{\rm eq}^{-}$

Eq. (52) can be arranged to

$$K_{\rm eq}^{-} = \frac{1}{2}Ml^2\left(\dot{\theta}_{\rm eq}^{-}\right)^2 = \frac{\Delta E^*}{1-\varepsilon}. \tag{58}$$

As supported by Eqs. (46) and (48), ΔE^* is a linear function of $\dot{\theta}_{\rm eq}^{-}$. Therefore, Eq. (58) is a quadratic equation of $\dot{\theta}_{\rm eq}^{-}$. By considering $\dot{\theta}_{\rm eq}^{-} > 0$, we can solve Eq. (58) for $\dot{\theta}_{\rm eq}^{-}$ as

$$\dot{\theta}_{\rm eq}^{-} = \frac{u_0 \cos\alpha \sinh(\omega T_{\rm set}) + \sqrt{F(u_0, T_{\rm set})}}{M\omega l^2 \sin^2\alpha}, \tag{59}$$

where F is a function of u_0 and $T_{\rm set}$ and can be arranged as a quadratic function of u_0 as follows.

$$F(u_0, T_{\rm set}) = \Gamma_2 u_0^2 + \Gamma_1 u_0 + \Gamma_0 \tag{60}$$

The coefficients in Eq. (60) are detailed as

$$\begin{aligned}
\Gamma_2 &= 2\left(\cosh(\omega T_{\rm set}) - 1\right)\sin^2\alpha + \cos^2\alpha \sinh^2(\omega T_{\rm set}), \\
\Gamma_1 &= -2Mgl(\alpha - 2\phi)\sin^2\alpha \sinh^2\left(\frac{\omega T_{\rm set}}{2}\right), \\
\Gamma_0 &= 2M^2 g^2 l^2 \alpha\phi \sin^2\alpha.
\end{aligned}$$

Eq. (60) is a parabola convex downward because Γ_2 is positive. Fig. 6 plots the value of F with respect to u_0 and $T_{\rm set}$ where the system parameters are chosen as $M = 1.0$ [kg], $l = 1.0$ [m] and $\phi = 0.10$ [rad]. We can confirm that F forms a parabola convex downward as a function of u_0. The minimum value of F becomes

$$F_{\min}(T_{\rm set}) = \frac{M^2 g^2 l^2 \sin^2\alpha G(T_{\rm set})}{8\left(2 + \cos^2\alpha\left(\cosh(\omega T_{\rm set}) - 1\right)\right)}, \tag{61}$$

where

$$\begin{aligned}
G(T_{\rm set}) = \alpha^2 + 20\alpha\phi + 4\phi^2 - \left(\alpha^2 - 12\alpha\phi + 4\phi^2\right)\cosh(\omega T_{\rm set}) \\
+2(\alpha + 2\phi)^2 \cos(2\alpha)\sinh^2\left(\frac{\omega T_{\rm set}}{2}\right).
\end{aligned} \tag{62}$$

The partial derivative of $F_{\min}(T_{\rm set})$ with respect to $T_{\rm set}$ becomes

$$\frac{\partial F_{\min}(T_{\rm set})}{\partial T_{\rm set}} = -\frac{2M^2 g^2 l^2 \omega(\alpha - 2\phi)^2 \sin^4\alpha \sinh(\omega T_{\rm set})}{\left(4 + 2\cos^2\alpha(\cosh(\omega T_{\rm set}) - 1)\right)^2} < 0. \tag{63}$$

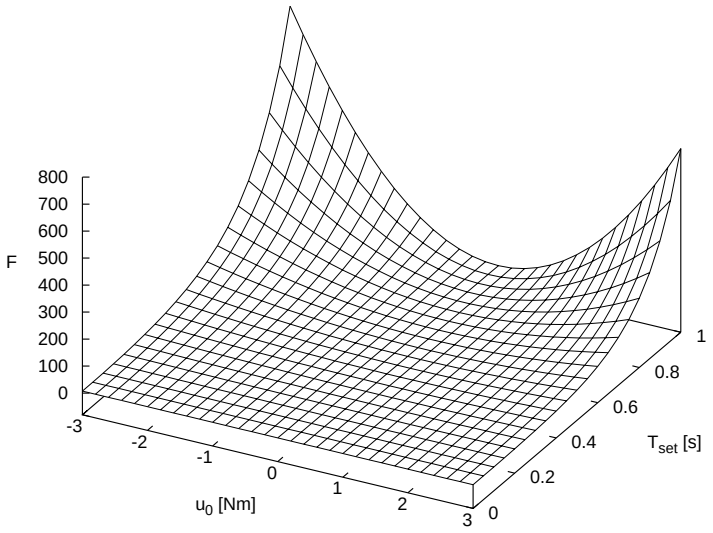

Fig. 6 F with respect to u_0 and $T_{\rm set}$ where $M = 1.0$ [kg], $l = 1.0$ [m] and $\phi = 0.10$ [rad]

Therefore, $F_{\rm min}(T_{\rm set})$ can be found to be a monotonically decreasing function. On the other hand, $F_{\rm min}(0)$ and $F_{\rm min}(\infty)$ become

$$F_{\rm min}(0) = 2M^2g^2l^2\alpha\phi\sin^2\alpha,$$
$$F_{\rm min}(\infty) = \frac{M^2g^2l^2}{8}\tan^2\alpha\left((\alpha+2\phi)^2\cos(2\alpha) - \alpha^2 + 12\alpha\phi - 4\phi^2\right).$$

$F_{\rm min}(\infty)$ can be factorized to

$$F_{\rm min}(\infty) = -M^2g^2l^2\tan^2\alpha\sin^2\alpha\left(\phi - \frac{\alpha}{2}\tan^2\frac{\alpha}{2}\right)\left(\phi - \frac{\alpha}{2}\cot^2\frac{\alpha}{2}\right), \quad (64)$$

and we can conclude

$$F_{\rm min}(\infty) > 0 \iff \frac{\alpha}{2}\tan^2\frac{\alpha}{2} < \phi < \frac{\alpha}{2}\cot^2\frac{\alpha}{2}. \quad (65)$$

This condition includes the inequality of Eq. (39), that is, $F_{\rm min}(T_{\rm set})$ can be determined if the walker can exhibit passive dynamic walking.

4.5 Analytical solution of $\bar{Q}$ and its accuracy

By substituting $\dot{\theta}^-_{\rm eq}$ of Eq. (59) into Eq. (56), $\bar{Q}$ can be derived as a function of u_0 and $T_{\rm set}$ as

$$\bar{Q}\left(u_0, T_{\rm set}\right) = \frac{u_0\sinh\left(\omega T_{\rm set}\right) + \cos\alpha\sqrt{F(u_0, T_{\rm set})}}{u_0\cos\alpha\sinh\left(\omega T_{\rm set}\right) + \sqrt{F(u_0, T_{\rm set})}}. \quad (66)$$

Again, in the case without actuation, i.e. passive dynamic walking, the following values can be derived from Eq. (66) by considering $F(0,0) = \Gamma_0 \neq 0$.

$$\bar{Q}\left(0, T_{\mathrm{set}}\right) = \cos\alpha, \quad \bar{Q}\left(u_0, 0\right) = \cos\alpha \tag{67}$$

In the following, we discuss the accuracy of $\bar{Q}$. Let us define the real transition function of the state error for the stance phase of the (i)th step, $\bar{Q}_i$, as

$$\bar{Q}_i := \frac{\Delta\dot{\theta}_{i+1}^{-}}{\Delta\dot{\theta}_i^{+}}. \tag{68}$$

Fig. 7 shows the evolution of $\bar{Q}_i$ with respect to the step number where $T_{\mathrm{set}} = 0.1$ [s], $u_0 = 1.0$ [s] and $\phi = 0.10$ [rad] in the linearized model and its magnified view. We can see that the value seems mostly unchanged for the initial steps but it begins to violate later. This is because the denominator of Eq. (68) converges to zero as well as the numerator, that is, Eq. (68) finally becomes an indeterminate form. Therefore we can take the values only for the first several steps for evaluation. As shown in the magnified view in Fig. 7, however, there are considerable changes in $\bar{Q}$ for the initial steps due to the nonlinearity of the real walking system. We then numerically compute the value of $\bar{Q}$ for the linearized and the nonlinear models as the mean value of $\bar{Q}$ for the first five steps:

$$\bar{Q} := \frac{1}{5}\sum_{i=0}^{4}\bar{Q}_i. \tag{69}$$

4.5.1 Effect of T_{set}

The partial derivative of $\bar{Q}$ with respect to T_{set} becomes significantly complicated but at $T_{\mathrm{set}} = 0$ it becomes the following simple function:

$$\left.\frac{\partial\bar{Q}\left(u_0, T_{\mathrm{set}}\right)}{\partial T_{\mathrm{set}}}\right|_{T_{\mathrm{set}}=0} = \frac{u_0\omega\sin\alpha}{\sqrt{2\alpha\phi Mgl}}. \tag{70}$$

Then the value of $\bar{Q}$ monotonically increases with the slight increase of T_{set} from zero if u_0 is positive. In other words, the convergence speed decreases by the effect of acceleration. As discussed in subsection 4.3, in this case $\bar{Q}$ becomes larger than $\bar{R}$.

Fig. 8 plots $\bar{Q}$ of Eq. (69) in the linear and the nonlinear models and the analytical solution of $\bar{Q}$ of Eq. (66) with respect to T_{set} where $u_0 = 1.0$ [N·m] and $\phi = 0.10$ [rad]. The initial angular velocity is chosen as $\dot{\theta}_0^{+} = \dot{\theta}_{\mathrm{eq}}^{+} + 0.01$ [rad/s]. We can see that the values of $\bar{Q}$ in all cases monotonically increase with the increase of T_{set} as theoretically shown and that the analytical solution shows a high degree of accuracy.

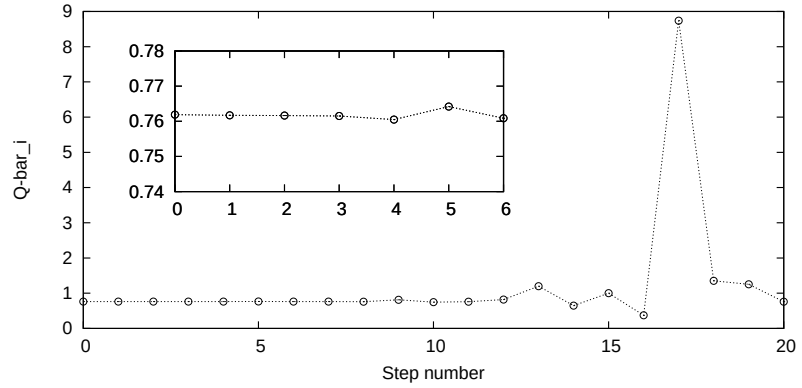

Fig. 7 Evolution of $\bar{Q}_i$ where $T_{\text{set}} = 0.1$ [s], $u_0 = 1.0$ [N·m] and $\phi = 0.10$ [rad]

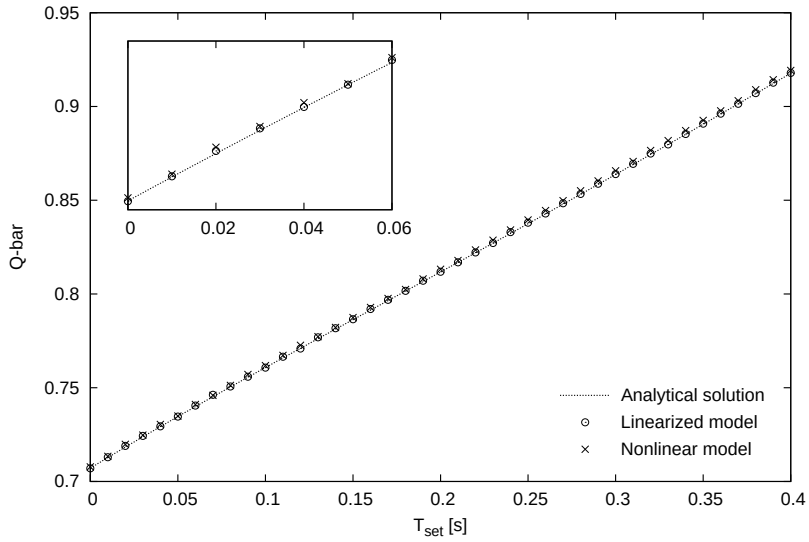

Fig. 8 $\bar{Q}$ versus T_{set} where $u_0 = 1.0$ [N·m] and $\phi = 0.10$ [rad]

4.5.2 Effect of u_0

The partial derivative of $\bar{Q}$ with respect to u_0 also becomes complicated but at $u_0 = 0$ it becomes the following simple function:

$$\left.\frac{\partial \bar{Q}\left(u_0, T_{\text{set}}\right)}{\partial u_0}\right|_{u_0=0} = \frac{\sin\alpha \sinh\left(\omega T_{\text{set}}\right)}{\sqrt{2\alpha\phi} M g l}. \tag{71}$$

Since Eq. (71) is always positive, the value of $\bar{Q}$ monotonically should increase as u_0 increases around zero.

Fig. 9 plots $\bar{Q}$ of Eq. (69) in the linear and the nonlinear models and the analytical solution of $\bar{Q}$ of Eq. (66) with respect to u_0 where $T_{\rm set} = 0.1$ [s] and $\phi = 0.10$ [rad]. The initial angular velocity is chosen as $\dot{\theta}_0^+ = \dot{\theta}_{\rm eq}^+ + 0.01$ [rad/s]. We can see that the analytical solution shows a high degree of accuracy and that $\bar{Q}$ monotonically increases as u_0 increases through $\cos(\pi/4) = 1/\sqrt{2} = 0.7071$ at $u_0 = 0$. Negative u_0 decreases the value of $\bar{Q}$ or increases the convergence speed, and positive u_0 has the opposite effect.

4.5.3 Effect of initial state error

Fig. 10 plots $\bar{Q}$ of Eq. (69) in the linear and the nonlinear models and the analytical solution of $\bar{Q}$ of Eq. (66) with respect to the initial state error, $\Delta\dot{\theta}_0^+$, where $T_{\rm set} = 0.1$ [s], $u_0 = 1.0$ [N·m] and $\phi = 0.1$ [rad]. The value of the analytical solution in this case is $\bar{Q} = 0.760761$. We calculated the numerical solutions increasing $\Delta\dot{\theta}_0^+$ by 0.005 [rad/s] and plotted the mean values together with the maximum and minimum values. We can see that the mean value or real $\bar{Q}$ monotonically increases with the increase of $\Delta\dot{\theta}_0^+$ where $\Delta\dot{\theta}_0^+ \geq 0.1$ [rad/s]. This reduction of accuracy comes from the system nonlinearity. With the increase of $\Delta\dot{\theta}_0^+$, it becomes increasingly difficult to assume that $\bar{Q}$ is constant. The magnitude of the error is, however, within 0.01 even if $\Delta\dot{\theta}_0^+$ increases up to 0.2 [rad] which is about 15% of $\dot{\theta}_{\rm 1eq}^+$. Therefore we can conclude that the analytical solution can provide a reasonable reference value of $\bar{Q}$. On the other hand, the magnitude of the error where $\Delta\dot{\theta}_0^+ = 0.005$ [rad/s] is larger

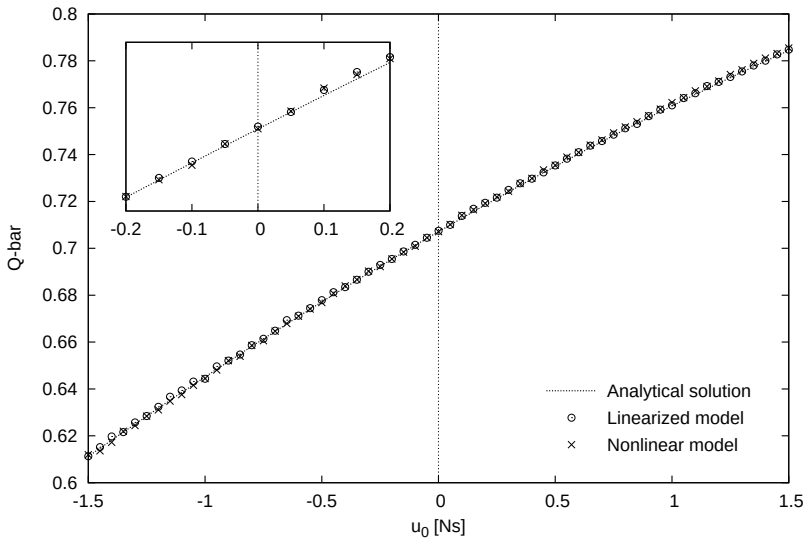

Fig. 9 $\bar{Q}$ versus u_0 where $T_{\rm set} = 0.1$ [s] and $\phi = 0.10$ [rad]

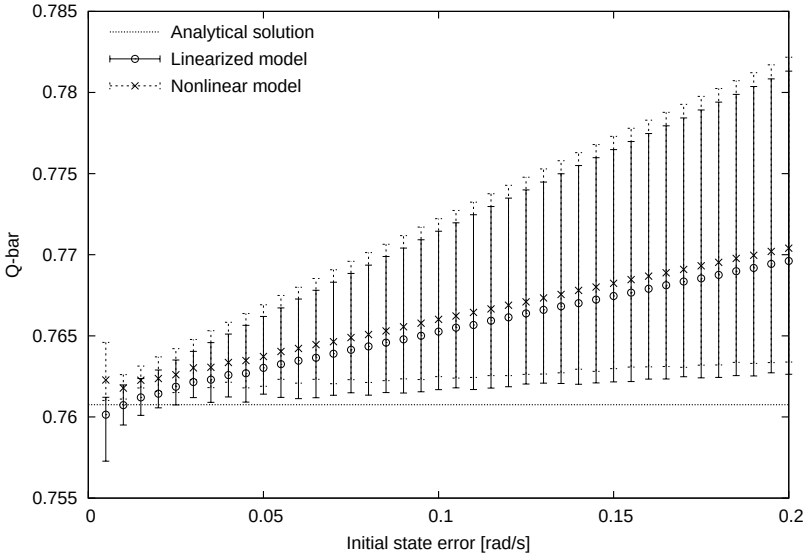

Fig. 10 $\bar{Q}$ versus initial state error where $T_{\mathrm{set}} = 0.1$ [s], $u_0 = 1.0$ [N·m] and $\phi = 0.1$ [rad]

than that where $\Delta\dot{\theta}_0^+ = 0.01$ [rad/s]. This is because the initial state error is very small and Eq. (69) converges to an indeterminate form after taking a few steps. This problem on numerical calculation arises in a fast convergent gait and is discussed again in the next section.

5 Extension to underactuated rimless wheel

This section discusses the discrete behavior of HZD of an underactuated rimless wheel (URW) with a torso in the same manner as the previous sections. The main purpose is to specify the analysis method with general formulae.

5.1 Model of underactuated rimless wheel and its linear approximate equation of motion

Fig. 11 shows the model of an URW with a torso [16]. This URW consists of an eight-legged symmetrically-shaped RW of Fig. 1 and a torso link. The torso link is connected to the RW at the central position and the moment of inertia about the joint is I [kg·m^2].

Let $\boldsymbol{\theta} = \begin{bmatrix}\theta_1 & \theta_2\end{bmatrix}^{\mathrm{T}}$ be the generalized coordinate vector. The equation of motion then becomes

$$\begin{bmatrix} Ml^2 & 0 \\ 0 & I \end{bmatrix} \begin{bmatrix} \ddot{\theta}_1 \\ \ddot{\theta}_2 \end{bmatrix} + \begin{bmatrix} -Mgl\sin\theta_1 \\ 0 \end{bmatrix} = \begin{bmatrix} 1 \\ -1 \end{bmatrix} u. \tag{72}$$

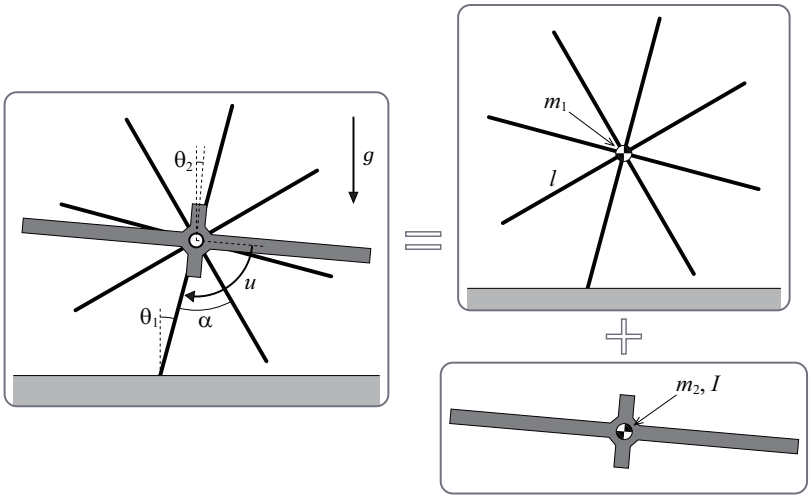

Fig. 11 Model of underactuated rimless wheel with torso

By linearizing Eq. (72) about $\boldsymbol{\theta} = \dot{\boldsymbol{\theta}} = \mathbf{0}_{2\times 1}$, we get

$$\begin{bmatrix} Ml^2 & 0 \\ 0 & I \end{bmatrix} \begin{bmatrix} \ddot{\theta}_1 \\ \ddot{\theta}_2 \end{bmatrix} + \begin{bmatrix} -Mgl & 0 \\ 0 & 0 \end{bmatrix} \begin{bmatrix} \theta_1 \\ \theta_2 \end{bmatrix} = \begin{bmatrix} 1 \\ -1 \end{bmatrix} u. \tag{73}$$

We denote Eq. (73) as

$$\boldsymbol{M}_0 \ddot{\boldsymbol{\theta}} + \boldsymbol{G}_0 \boldsymbol{\theta} = \boldsymbol{S} u. \tag{74}$$

Next, we outline the collision dynamics. We assume the followings.

- The URW falls down as a 1-DOF rigid body or achieves the condition of $\dot{\theta}_1 = \dot{\theta}_2$ immediately before the next impact.
- The torso is mechanically locked to the RW during the collision. The velocity constraint condition is mathematically represented by $\dot{\theta}_1^+ = \dot{\theta}_2^+$.

On the above assumptions, the transition equation for the angular velocity at the (i)th impact becomes

$$\dot{\theta}_{1(i)}^+ = \dot{\theta}_{2(i)}^+ = \frac{Ml^2 \cos\alpha + I}{Ml^2 + I} \dot{\theta}_{1(i)}^-. \tag{75}$$

Under this condition, a strict output following control can be achieved as described later. On the other hand, in a steady gait the following relation holds.

$$\dot{\theta}_{1\mathrm{eq}}^+ = \dot{\theta}_{2\mathrm{eq}}^+ = \bar{R} \dot{\theta}_{1\mathrm{eq}}^-, \quad \bar{R} := \frac{Ml^2 \cos\alpha + I}{Ml^2 + I} \tag{76}$$

By subtracting Eq. (76) from Eq. (75), we get $\Delta\dot{\theta}_{1(i)}^+ = \bar{R} \Delta\dot{\theta}_{1(i)}^-$ where $\Delta\dot{\theta}_{1(i)}^\pm := \dot{\theta}_{1(i)}^\pm - \dot{\theta}_{1\mathrm{eq}}^\pm$. Therefore $\bar{R}$ is found to be the transition function of the state error for the collision phase, and we can understand that this phase is stable because $\left|\bar{R}\right| < 1$ holds.

5.2 Quadratic approximation of mechanical energy

Define the potential energy corresponding to the linearized model as

$$P(\boldsymbol{\theta}) = P_{\max} + \frac{1}{2}\boldsymbol{\theta}^{\mathrm{T}}\boldsymbol{G}_0\boldsymbol{\theta}, \tag{77}$$

where $P_{\max} = Mgl$ [J] is the maximum potential energy the URW can reach. Eq. (77) is a quadratic approximation of potential energy for the nonlinear model. The kinetic energy is also determined as

$$K(\dot{\boldsymbol{\theta}}) = \frac{1}{2}\dot{\boldsymbol{\theta}}^{\mathrm{T}}\boldsymbol{M}_0\dot{\boldsymbol{\theta}}, \tag{78}$$

and this is common to both the nonlinear and the linearized models because the inertia matrix is constant. The total mechanical energy corresponding to the linearized model is then defined as

$$E(\boldsymbol{x}) := K(\dot{\boldsymbol{\theta}}) + P(\boldsymbol{\theta}) = P_{\max} + \frac{1}{2}\boldsymbol{x}^{\mathrm{T}}\boldsymbol{W}_0\boldsymbol{x}, \tag{79}$$

where

$$\boldsymbol{W}_0 := \begin{bmatrix} \boldsymbol{G}_0 & \boldsymbol{0}_{2\times 2} \\ \boldsymbol{0}_{2\times 2} & \boldsymbol{M}_0 \end{bmatrix} \in \mathbb{R}^{4\times 4}, \quad \boldsymbol{x} = \begin{bmatrix} \boldsymbol{\theta} \\ \dot{\boldsymbol{\theta}} \end{bmatrix} \in \mathbb{R}^4.$$

$\boldsymbol{W}_0$ is a symmetric matrix and the time-derivative of $E(\boldsymbol{x})$ becomes

$$\frac{\mathrm{d}E(\boldsymbol{x})}{\mathrm{d}t} = \boldsymbol{x}^{\mathrm{T}}\boldsymbol{W}_0\dot{\boldsymbol{x}} = \dot{\boldsymbol{\theta}}^{\mathrm{T}}\left(\boldsymbol{G}_0\boldsymbol{\theta} + \boldsymbol{M}_0\ddot{\boldsymbol{\theta}}\right) = \dot{\boldsymbol{\theta}}^{\mathrm{T}}\boldsymbol{S}u. \tag{80}$$

Therefore, the principle of conservation of mechanical energy is reproduced in the linearized system. Unlike the case of the active RW, in the derivation of Eq. (80) we did not use the state space representation because in this case $\boldsymbol{A}$ and $\boldsymbol{B}$ are defined in a different meaning after input-output linearization as described later.

5.3 Output following control and typical walking gait

Let $y := \boldsymbol{S}^{\mathrm{T}}\boldsymbol{\theta} = \theta_1 - \theta_2$ be the control output. We then consider to control y from $-\alpha/2$ to $\alpha/2$ during every stance phase by strictly tracking to the following desired-time trajectory.

$$y_{\mathrm{d}}(t) = \begin{cases} \dfrac{6\alpha}{T_{\mathrm{set}}^5}t^5 - \dfrac{15\alpha}{T_{\mathrm{set}}^4}t^4 + \dfrac{10\alpha}{T_{\mathrm{set}}^3}t^3 - \dfrac{\alpha}{2} & (0 \le t < T_{\mathrm{set}}) \\ \dfrac{\alpha}{2} & (t \ge T_{\mathrm{set}}) \end{cases} \tag{81}$$

This satisfies the following boundary conditions.

$$y_{\mathrm{d}}(0^+) = -\frac{\alpha}{2},\ y_{\mathrm{d}}(T_{\mathrm{set}}) = \frac{\alpha}{2},\ \dot{y}_{\mathrm{d}}(0^+) = \dot{y}_{\mathrm{d}}(T_{\mathrm{set}}) = 0,\ \ddot{y}_{\mathrm{d}}(0^+) = \ddot{y}_{\mathrm{d}}(T_{\mathrm{set}}) = 0$$

By choosing the conditions immediately after impact as $\theta_1^+ = -\alpha/2$, $\theta_2^+ = 0$ and $\dot{\theta}_1^+ = \dot{\theta}_2^+$, we can achieve $y(0^+) = y_\mathrm{d}(0^+)$, $\dot{y}(0^+) = \dot{y}_\mathrm{d}(0^+)$ and $\ddot{y}(0^+) = \ddot{y}_\mathrm{d}(0^+)$. Therefore the URW can strictly control y without including the tracking errors, and PD feedback control is not necessary. The second-order derivative of y with respect to time becomes $\ddot{y} = \boldsymbol{S}^\mathrm{T}\ddot{\boldsymbol{\theta}} = \boldsymbol{S}^\mathrm{T}\boldsymbol{M}_0^{-1}\left(\boldsymbol{S}u - \boldsymbol{G}_0\boldsymbol{\theta}\right)$, and the control input, u, for achieving $\ddot{y} = \ddot{y}_\mathrm{d}(t)$, i.e. $y \equiv y_\mathrm{d}(t)$, can be determined as

$$u = \frac{\ddot{y}_\mathrm{d}(t) + \boldsymbol{S}^\mathrm{T}\boldsymbol{M}_0^{-1}\boldsymbol{G}_0\boldsymbol{\theta}}{\boldsymbol{S}^\mathrm{T}\boldsymbol{M}_0^{-1}\boldsymbol{S}} = \frac{Ml^2 I}{Ml^2 + I}\left(\ddot{y}_\mathrm{d}(t) - \omega^2\theta_1\right), \tag{82}$$

where $\omega := \sqrt{g/l}$ [rad/s]. By substituting this into Eq. (73) and extracting the first row, we get

$$\ddot{\theta}_1 = \hat{\omega}^2\theta_1 + \frac{I}{Ml^2 + I}\ddot{y}_\mathrm{d}(t), \quad \hat{\omega} := \omega\sqrt{\frac{Ml^2}{Ml^2 + I}}. \tag{83}$$

The state-space realization of Eq. (83) then becomes

$$\frac{\mathrm{d}}{\mathrm{d}t}\begin{bmatrix}\theta_1 \\ \dot{\theta}_1\end{bmatrix} = \begin{bmatrix}0 & 1 \\ \hat{\omega}^2 & 0\end{bmatrix}\begin{bmatrix}\theta_1 \\ \dot{\theta}_1\end{bmatrix} + \begin{bmatrix}0 \\ I/(Ml^2 + I)\end{bmatrix}\ddot{y}_\mathrm{d}(t). \tag{84}$$

In the following, we denote Eq. (84) as

$$\dot{\boldsymbol{x}} = \boldsymbol{A}\boldsymbol{x} + \boldsymbol{B}\ddot{y}_\mathrm{d}(t). \tag{85}$$

The linearized equation of motion in this case is also specified as a linear time-invariant system with a steady control input, $\ddot{y}_\mathrm{d}(t)$, as with the previous case. The arranged dynamics of Eq. (83) is equivalent to the linearized dynamics of a RW whose inertia is $Ml^2 + I$ and control input is $I\ddot{y}_\mathrm{d}(t)$.

Fig. 12 shows the simulation results of the steady level dynamic walking where $T_\mathrm{set} = 0.7$ [s]. Here, (a) shows the angular positions and the control output in the nonlinear model and (b) shows those in the linearized model. We can see that the strict output-following control is achieved and that the linearized model generates stationary orbits very close to those of the nonlinear model.

Fig. 13 shows the time evolutions of the total mechanical energy in the nonlinear model and $E(\boldsymbol{x})$ in the linearized model. We can see that $E(\boldsymbol{x})$ generates a stationary orbit very close to that of the nonlinear model. This is because the only difference between the mechanical energy and $E(\boldsymbol{x})$ is the difference between the potential energies. In every stance phase, from 0 to $T_\mathrm{set}/2$, mechanical energy increases because the control torque accelerates the RW and torso. Whereas from $T_\mathrm{set}/2$ to T_set, mechanical energy decreases due to deceleration effect. After that, the URW moves as a 1-DOF rigid body and the mechanical energy is maintained constant.

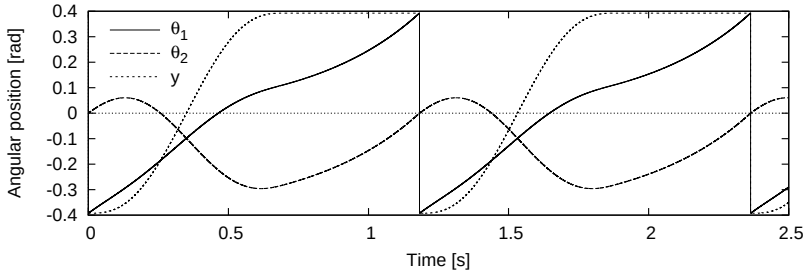

(a) Nonlinear model

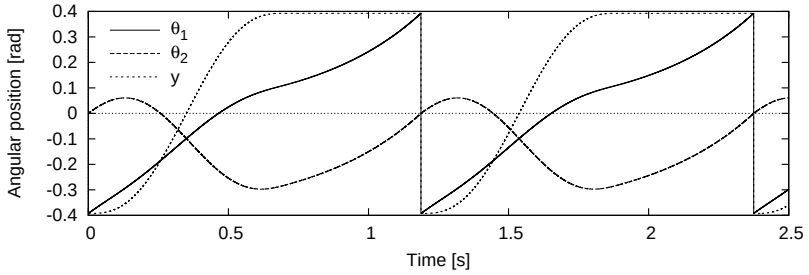

(b) Linearized model

Fig. 12 Time evolutions of angular positions and control output in nonlinear and linearized models

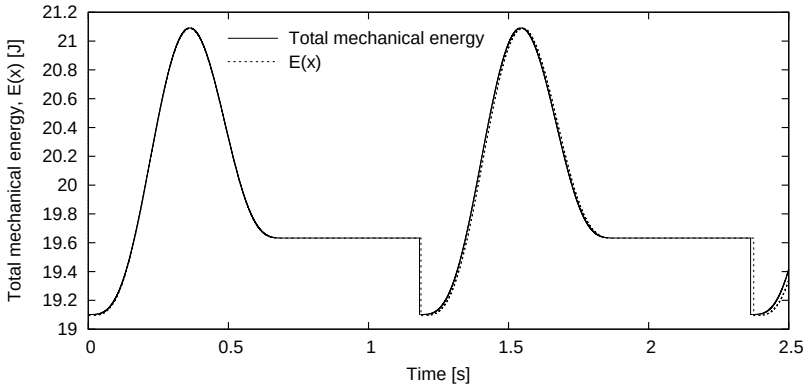

Fig. 13 Time evolutions of total mechanical energy and $E(\boldsymbol{x})$

5.4 Derivations of $\dot{\theta}_{1\mathrm{eq}}^{-}$, ΔE_i and $\bar{Q}$

The kinetic energy immediately before impact of the URW also satisfies the following recurrence formula:

$$K_{i+1}^{-} = \varepsilon K_i^{-} + \Delta E_i, \tag{86}$$

and the steady equation becomes

$$K_{\mathrm{eq}}^{-} = \varepsilon K_{\mathrm{eq}}^{-} + \Delta E^{*} \iff K_{\mathrm{eq}}^{-} = \frac{\Delta E^{*}}{1-\varepsilon}. \tag{87}$$

The energy-loss coefficient in this case, however, satisfies

$$\varepsilon := \frac{K_i^{+}}{K_i^{-}} = \frac{\frac{1}{2} I' \left(\dot{\theta}_{1(i)}^{+}\right)^2}{\frac{1}{2} I' \left(\dot{\theta}_{1(i)}^{-}\right)^2} = \left(\frac{\dot{\theta}_{1(i)}^{+}}{\dot{\theta}_{1(i)}^{-}}\right)^2 = \bar{R}^2, \tag{88}$$

where $I' := Ml^2 + I$ [kg·m^2] is the total moment of inertia about the stance-leg end. Eq. (87) can be equivalently arranged to

$$H\left(\dot{\theta}_{1\mathrm{eq}}^{-}\right) := (1-\varepsilon) K_{\mathrm{eq}}^{-} - \Delta E^{*} = 0. \tag{89}$$

The function H can be expressed as a quadratic equation of $\dot{\theta}_{1\mathrm{eq}}^{-}$ as follows.

$$H\left(\dot{\theta}_{1\mathrm{eq}}^{-}\right) = C_2 \left(\dot{\theta}_{1\mathrm{eq}}^{-}\right)^2 + C_1 \dot{\theta}_{1\mathrm{eq}}^{-} + C_0 = 0 \tag{90}$$

Here, note that K_{eq}^{-} is a quadratic equation of $\dot{\theta}_{1\mathrm{eq}}^{-}$ and ΔE^{*} is a linear function of it, that is, the following relations hold.

$$(1-\varepsilon) K_{\mathrm{eq}}^{-} = C_2 \left(\dot{\theta}_{1\mathrm{eq}}^{-}\right)^2, \quad \Delta E^{*} = -C_1 \dot{\theta}_{1\mathrm{eq}}^{-} - C_0 \tag{91}$$

$\dot{\theta}_{1\mathrm{eq}}^{-}$ is then derived as the solution of $H\left(\dot{\theta}_{1\mathrm{eq}}^{-}\right) = 0$, that is,

$$\dot{\theta}_{1\mathrm{eq}}^{-} = \frac{-C_1 + \sqrt{C_1^2 - 4C_2 C_0}}{2C_2}. \tag{92}$$

The quadratic equation (90) has another solution of $\dot{\theta}_{1\mathrm{eq}}^{-}$, but this is negative and improper.

Let t [s] be the time parameter which is reset to zero at every impact. The state vector for $0^{+} \le t \le T_{\mathrm{set}}$, $\boldsymbol{x}(t) \in \mathbb{R}^2$, is then determined as

$$\boldsymbol{x}(t) = \mathrm{e}^{\boldsymbol{A}t} \boldsymbol{x}_i^{+} + \int_{0^{+}}^{t} \mathrm{e}^{\boldsymbol{A}(t-s)} \boldsymbol{B} \ddot{y}_{\mathrm{d}}(s) \mathrm{d}s. \tag{93}$$

$\theta_1(t)$ is then obtained by extracting the first element of $\boldsymbol{x}(t)$ in Eq. (93). By considering the following relation:

$$\frac{\mathrm{d}E(\boldsymbol{x})}{\mathrm{d}t} = \dot{\boldsymbol{\theta}}^{\mathrm{T}} \boldsymbol{S} u(t) = \dot{y}(t) u(t) = \dot{y}_{\mathrm{d}}(t) u(t), \tag{94}$$

we can calculate the restored mechanical energy as follows.

$$\Delta E_i = \int_{0^{+}}^{T_{\mathrm{set}}} \dot{y}_{\mathrm{d}}(s) u(s) \, \mathrm{d}s = \frac{I\hat{\omega}^2}{\omega^2} \int_{0^{+}}^{T_{\mathrm{set}}} \dot{y}_{\mathrm{d}}(s) \left(\ddot{y}_{\mathrm{d}}(s) - \omega^2 \theta_1(s)\right) \mathrm{d}s \tag{95}$$

Here, we can obtain the following.

$$\int_{0^+}^{T_{\rm set}} \dot{y}_{\rm d}(s)\ddot{y}_{\rm d}(s){\rm d}s = \left[\frac{1}{2}\dot{y}_{\rm d}(s)^2\right]_{s=0^+}^{s=T_{\rm set}} = 0$$

Eq. (95) then becomes

$$\Delta E_i = -I\hat{\omega}^2 \int_{0^+}^{T_{\rm set}} \dot{y}_{\rm d}(s)\theta_1(s)\ {\rm d}s. \tag{96}$$

The restored mechanical energy is therefore found to be the integral of the product of $\dot{y}_{\rm d}(t)$ and the zero dynamics, $\theta_1(t)$. Note that $\theta_1(t)$ is given as a linear function of $\dot{\theta}^+_{1(i)}$, and so is ΔE_i. Specifically, ΔE_i is determined as

$$\begin{aligned}\Delta E_i &= -C_1\dot{\theta}^-_{1(i)} - C_0 = -C_1\left(\dot{\theta}^-_{1\rm eq} + \Delta\dot{\theta}^-_{1(i)}\right) - C_0 \\ &= \Delta E^* - C_1\Delta\dot{\theta}^-_{1(i)}.\end{aligned} \tag{97}$$

Note that we used the relation $\Delta E^* = -C_1\dot{\theta}^-_{1\rm eq} - C_0$.

The kinetic energy immediately before the (i)th impact can be approximated as follows.

$$\begin{aligned}K^-_i &= \frac{1}{2}I'\left(\dot{\theta}^-_{1(i)}\right)^2 = \frac{1}{2}I'\left(\dot{\theta}^-_{1\rm eq} + \Delta\dot{\theta}^-_{1(i)}\right)^2 \approx \frac{1}{2}I'\left(\left(\dot{\theta}^-_{1\rm eq}\right)^2 + 2\dot{\theta}^-_{1\rm eq}\Delta\dot{\theta}^-_{1(i)}\right) \\ &= K^-_{\rm eq} + I'\dot{\theta}^-_{1\rm eq}\Delta\dot{\theta}^-_{1(i)}\end{aligned} \tag{98}$$

The recurrence formula (86) is then represented as follows.

$$K^-_{\rm eq} + I'\dot{\theta}^-_{1\rm eq}\Delta\dot{\theta}^-_{1(i+1)} = \varepsilon\left(K^-_{\rm eq} + I'\dot{\theta}^-_{1\rm eq}\Delta\dot{\theta}^-_{1(i)}\right) + \Delta E^* - C_1\Delta\dot{\theta}^-_{1(i)} \tag{99}$$

By subtracting Eq. (87) from Eq. (99), we get

$$I'\dot{\theta}^-_{1\rm eq}\Delta\dot{\theta}^-_{1(i+1)} = \varepsilon I'\dot{\theta}^-_{1\rm eq}\Delta\dot{\theta}^-_{1(i)} - C_1\Delta\dot{\theta}^-_{1(i)}, \tag{100}$$

and this is arranged to

$$\Delta\dot{\theta}^-_{1(i+1)} = \left(\varepsilon - \frac{C_1}{I'\dot{\theta}^-_{1\rm eq}}\right)\Delta\dot{\theta}^-_{1(i)}. \tag{101}$$

This means

$$\bar{Q}\bar{R} = \varepsilon - \frac{C_1}{I'\dot{\theta}^-_{1\rm eq}}. \tag{102}$$

Considering $\varepsilon = \bar{R}^2$ and $\dot{\theta}^+_{1\rm eq} = \bar{R}\dot{\theta}^-_{1\rm eq}$, Eq. (102) can be arranged to

$$\bar{Q} = \bar{R} - \frac{C_1}{I'\dot{\theta}^+_{1\rm eq}}. \tag{103}$$

This is a general formulation of $\bar{Q}$ and specifies the relationship between the convergence properties of the stance and collision phases. Note that the relationship $\bar{Q} = \bar{R}$ holds if $C_1 = 0$. In other words, the convergence properties of the both phases become identical in the case that the restored mechanical energy is constant. This supports the results in the previous sections. Fully-actuated bipedal walkers can achieve $C_1 = 0$ and discretely behave as a passive RW [8,9]. Underactuated bipedal walkers, however, cannot achieve it in general.

5.5 Analysis results

Fig. 14 plots the analytical $\bar{Q}$ and the numerical ones for the linearized and the nonlinear models with respect to $T_{\rm set}$ where $M = 2.0$ [kg], $l = 1.0$ [m], $I = 1.0$ [kg·m^2]. The initial angular velocity is chosen as $\dot{\theta}^+_{1(0)} = \dot{\theta}^+_{1\rm eq} + 0.01$ [rad/s]. Considering that the generated gait in this case converges faster than that in semi-passive dynamic walking, we numerically compute the value of $\bar{Q}$ for the linearized and the nonlinear models as the mean value of $\bar{Q}$ for the first three steps:

$$\bar{Q} := \frac{1}{3}\sum_{i=0}^{2} \bar{Q}_i. \tag{104}$$

From the result, we can see that the accuracy of the analytical $\bar{Q}$ is sufficiently high and the numerical ones tend to diverge near the deadbeat mode. As in the case of an underactuated biped [13], the convergence property changes

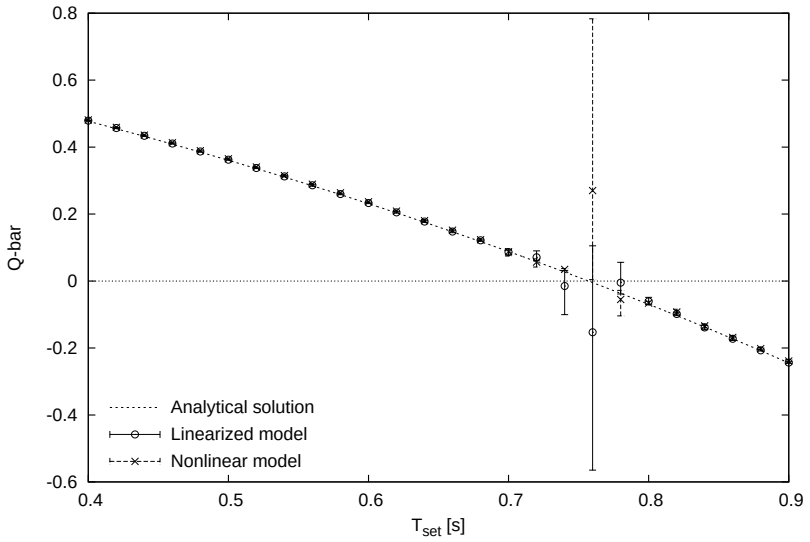

Fig. 14 $\bar{Q}$ and its numerical solutions versus $T_{\rm set}$

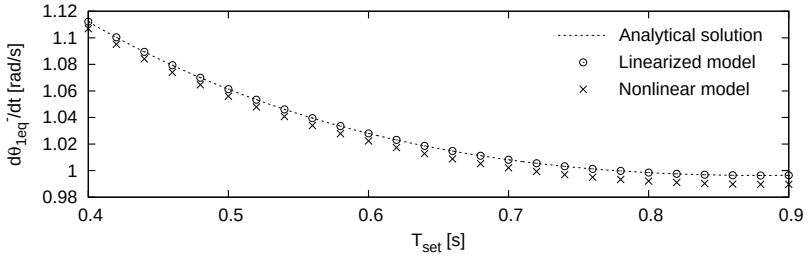

Fig. 15 $\dot{\theta}^{-}_{1\mathrm{eq}}$ and its numerical solutions versus T_{set}

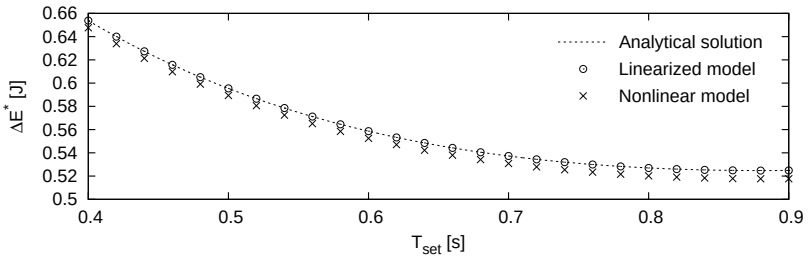

Fig. 16 $\dot{\theta}^{-}_{1\mathrm{eq}}$ and its numerical solutions versus T_{set}

from the speed mode to the totter mode through the deadbeat mode as T_{set} increases.

Fig. 15 plots the analytical $\dot{\theta}^{-}_{1\mathrm{eq}}$ and the numerical ones for the linearized and the nonlinear models with respect to T_{set} in the previous result. We can see that the analytical $\dot{\theta}^{-}_{1\mathrm{eq}}$ is equal to the linearized one and that it shows a high degree of accuracy in comparison to the nonlinear one. Fig. 16 plots the analytical ΔE^{*} and the numerical ones for the linearized and the nonlinear models with respect to T_{set} in the previous result. We can also see that the analytical ΔE^{*} shows a high degree of accuracy. It is not clear yet that existence of the solution $\dot{\theta}^{-}_{1\mathrm{eq}}$ is equivalent to the condition for overcoming the potential barrier at mid-stance. More mathematical investigations are necessary.

6 Conclusion and future work

In this paper, we proposed a method for deriving fully analytical transition functions of the state error in limit cycle walking with constraint on impact posture and discussed how the convergence property changes according to the control parameters. We mathematically showed that use of quadratic approximation of mechanical energy in conjunction with linear approximate equation of motion enables to derive the restored mechanical energy, ΔE_i, as a linear function of $\Delta\dot{\theta}^{-}_{i}$, and that the transition function for the stance phase $\bar{Q}$ can

be simply specified denoting a relationship to that for the collision phase, $\bar{R}$. The greatest contribution of this paper to have established the stability analysis method independent of numerical integration for limit cycle walkers with constraint on impact posture. According to the method, numerical simulations are no longer needed to determine the limit cycle stability. The next subject is to deeply understand the mechanical implication and changing property of the fully analytical transition functions.

For further theory establishment, the following subjects are yet to be investigated in the future. Extension of the analysis method to general walkers with multiple-DOF is theoretically possible but the symbolic calculation load would become significantly heavy. Some realistic solutions for simplified calculation should be investigated. In general walkers, it is also an unavoidable problem that linearization of the inertia matrix causes non-negligible errors in the kinetic and potential energies. The calculation accuracy must be discussed.

Acknowledgements This research was partially supported by a Grant-in-Aid for Scientific Research, (C) No. 24560542, provided by the Japan Society for the Promotion of Science (JSPS).

References

1. Westervelt E. R., Grizzle, J.W., Chevallereau, C., Choi, J. H., Morris, B.: Feedback Control of Dynamic Bipedal Robot Locomotion, CRC Press (2007)
2. Wisse M., van der Linde, R. Q.: Delft Pneumatic Bipeds, Springer (2007)
3. Westervelt, E. R. Grizzle, J. W., Koditschek, D. E.: Hybrid zero dynamics of planar biped walkers, IEEE Trans. on Automatic Control, Vol. 48, No. 1, pp. 42–56 (2003)
4. McGeer, T.: Passive dynamic walking, Int. J. of Robotics Research, Vol. 9, No. 2, pp. 62–82 (1990)
5. McGeer, T.: Passive walking with knees, Proc. of the IEEE Int. Conf. on Robotics and Automation, Vol. 3, pp. 1640–1645 (1990)
6. Coleman, M. J., Chatterjee, A., Ruina, A.: Motions of a rimless spoked wheel: a simple three-dimensional system with impacts, Dynamics and Stability of Systems, Vol. 12, Iss. 3, pp. 139–159 (1997)
7. Coleman, M. J.: Dynamics and stability of a rimless spoked wheel: a simple 2D system with impacts, Dynamical Systems, Vol. 25, Iss. 2, pp. 215–238 (2010)
8. Asano, F., Luo, Z.-W.: Asymptotically stable biped gait generation based on stability principle of rimless wheel," Robotica, Vol. 27, Iss. 6, pp. 949–958 (2009)
9. Asano, F.: Efficiency and optimality of two-period limit cycle walking, Advanced Robotics, Vol. 26, No. 1–2, pp. 155–176 (2012)
10. Hosoe, S., Takeichi, K., Kumai, S., Ito, M.: Analysis of stability of dynamic biped locomotion with high gain feedback, Trans. of the Society of Instrument and Control Engineers, Vol. 22, No. 9, pp. 948–954 (1986) (In Japanese)
11. Grizzle, J. W., Abba, G., Plestan, F.: Asymptotically stable walking for biped robots: Analysis via systems with impulse effects, IEEE Trans. on Automatic Control, Vol. 46, No. 1, pp. 51–64 (2001)
12. Asano, F.: Stability analysis of underactuated bipedal gait using linearized model, Proc. of the 11th IEEE-RAS Int. Conf. on Humanoid Robots, pp. 282–287 (2011)
13. Asano, F.: Stability analysis of underactuated compass gait based on linearization of motion, Multibody System Dynamics, published as an online first view article. doi:10.1007/s11044-014-9416-9
14. Asano, F.: High-speed dynamic gait generation for limit cycle walkers based on forward-tilting impact posture, Multibody System Dynamics, Vol. 30, Iss. 3, pp. 287–310 (2013)

15. Asano, F., Xiao, X.: Role of deceleration effect in efficient and fast convergent gait generation, Proc. of the IEEE Int. Conf. on Robotics and Automation, pp. 5649–5654 (2013)
16. Asano, F., Xiao, X.: Output deadbeat control approaches to fast convergent gait generation of underactuated spoked walker, Proc. of the 2012 IEEE/SICE Int. Symp. on System Integration, pp. 265–270 (2012)